

# Unusual Cosmic Ray Variations During the Forbush Decreases of June 2015

E. Samara<sup>1</sup>  · A. Smponias<sup>1</sup> · I. Lytrosyngounis<sup>1</sup> ·  
D. Lingri<sup>1</sup> · H. Mavromichalaki<sup>1</sup> · C. Sgouropoulos<sup>1</sup>

Received: 16 October 2017 / Accepted: 29 March 2018 / Published online: 11 April 2018  
© Springer Science+Business Media B.V., part of Springer Nature 2018

**Abstract** Although the current Solar Cycle 24 is characterized by low solar activity, an intense geomagnetic storm (G4) was recorded in June 2015. It was a complex phenomenon that began on 22 June 2015 as the result of intense solar activity, accompanied by several flares and coronal mass ejections that interacted with the Earth's magnetic field. A Forbush decrease was also recorded at the neutron monitors of the worldwide network, with an amplitude of 8.4%, and in its recovery phase, a second Forbush decrease followed, with an amplitude of 4.0% for cosmic rays of 10 GV obtained with the global survey method. The Dst index reached a minimum value of  $-204$  nT that was detected on 23 June 2015 at 05:00–06:00 UT, while the Kp index reached the value eight. For our analysis, we used hourly cosmic-ray intensity data recorded by polar, mid-, and high-latitude neutron monitor stations obtained from the High Resolution Neutron Monitor Database. The cosmic-ray anisotropy variation at the ecliptic plane was also estimated and was found to be highly complex. We study and discuss the unusual and complex cosmic-ray and geomagnetic response to these solar events.

**Keywords** Solar activity · Cosmic ray intensity · Forbush decrease · Neutron monitors · Geomagnetic activity

## 1. Introduction

Forbush decreases (FDs) of cosmic-ray intensity and geomagnetic storms (GSs) recorded at Earth are an important aspect of space weather. Forbush decrease precursors can be used for space weather predictions (Kudela *et al.*, 2000; Badruddin, 2006; Papailiou *et al.*, 2012). FDs are generally believed to be produced by interplanetary coronal mass ejections (ICMEs) from the Sun (Venkatesan and Badruddin, 1990; Cane, 2000; Kumar and Badruddin, 2014, and references therein) which can also cause strong GSs. Although both FDs and GSs can

---

✉ H. Mavromichalaki  
emavromi@phys.uoa.gr

<sup>1</sup> Faculty of Physics, National and Kapodistrian University of Athens, 15784 Athens, Greece

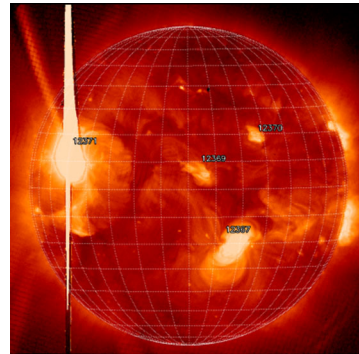
originate from a common solar and interplanetary disturbance, their magnitudes are not always proportional (Lingri *et al.*, 2016; Aslam and Badruddin, 2017).

The observed variations in the geomagnetic indices indicate that a GS has occurred. During a GS period and before the main phase, the development of auroral currents is recorded. The AE-index, originally introduced as the auroral electrojet index, is used as a measure of the electrojet activity caused by ionospheric currents that is detected as a disturbance in the auroral zone magnetometers (Davis and Sugiura, 1966). The Dst index is derived from equatorial and mid-latitude station magnetograms and indicates the geomagnetic activity. In a GS, the magnetospheric ring current intensity perturbs the horizontal magnetic component, and therefore the Dst index characterizes the intensity of the storm (Sugiura, 1964). There is an average time delay of about three hours between the commencement periods and also between the maximum values of the two indices (Akasofu *et al.*, 1983; Gonzalez *et al.*, 1994). In addition to the Dst index, we here used also the SYM-H index as a GS intensity measure. These indices lead to similar results, although they are derived from different processes. SYM-H index data provide us with high time resolution of about one minute, instead of the Dst data, which have a time resolution of one hour (Wanliss and Showalter, 2006; Tsurutani and Lakhina, 2014). The SYM-H index is derived from magnetometers just like the Dst-index, but it corresponds to the horizontal symmetric component of the geomagnetic field. Specifically, the term “symmetric” refers to the uniform field that was created from the ring current and is parallel to the resulting magnetic dipole direction (Wanliss and Showalter, 2006). The Kp index is also an index that indicates the intensity of GSs. In this case, the data are obtained from a network of 13 standard stations as a mean value of the two horizontal magnetic field disturbance components (Bartels, 1949).

At the declining phase of Solar Cycle 23, several strong solar and cosmic-ray (CR) events characterized by rather peculiar properties occurred in October–November 2003, January 2005, August–September 2005, and December 2006, for instance (Eroshenko *et al.*, 2004; Belov *et al.*, 2005; Plainaki *et al.*, 2007). Although the current Solar Cycle 24 is characterized by low solar activity, several of these extreme events occurred not only during the maximum, but also at the declining phase of this cycle, such as those in March 2012, May 2012, March 2015, June 2015, and September 2017 (Papaioannou *et al.*, 2014; Livada, Lingri, and Mavromichalaki, 2015; Kamide and Kusano, 2015; Aslam and Badruddin, 2017). During these events, dynamic phenomena related to solar flares and coronal mass ejections (CMEs) resulted in large variations in CR intensity up to energies of at least tens of GeV. Many studies have been published in order to explain the connection between solar phenomena and their impact on CRs (Harrison, 1995; Hundhausen, 1999; Cane, 2000; Kudela and Brenkus, 2004; Belov *et al.*, 2005; Mavromichalaki *et al.*, 2007). These studies show that extreme solar events influence CRs in a dynamic way, resulting in steep intensity decreases, such as FD, or increases, such as ground-level enhancements (GLEs). Different relations between CR variations and various parameters of solar wind and interplanetary space can be established (Belov *et al.*, 2001), such as the time lag and the behavioral comparison between the FDs and the Dst index (Aslam and Badruddin, 2017).

We here analyze the period of June 2015, which is characterized by substantial CME activity, with some of their interplanetary counterparts reaching Earth and resulting in a series of FDs. With our detailed study of the solar, interplanetary, CR, and geomagnetic conditions during the complex geoeffective event in June 2015, we aim to improve our understanding of the solar-terrestrial relations.

**Figure 1** Active region AR 2371 that produced the flares of interest ([https://www.solarmonitor.org/full\\_disk.php?date=20150619&type=hxrt\\_filter&indexnum=1](https://www.solarmonitor.org/full_disk.php?date=20150619&type=hxrt_filter&indexnum=1)).



## 2. Data Selection

In order to study this event globally, data from various sources were used. The CME first appearance time as observed by the *C2 Large Angle and Spectroscopic Coronagraph* (LASCO) of the *Solar and Heliospheric Observatory* (SOHO) were obtained from the SOHO/LASCO CME Catalog ([https://cdaw.gsfc.nasa.gov/CME\\_list/](https://cdaw.gsfc.nasa.gov/CME_list/)), while data for the CME shock arrival times at Earth were taken from the NASA CME Arrival Time Scoreboard (<https://kauai.ccmc.gsfc.nasa.gov/CMEscoreboard/PreviousPredictions/2015;jsessionid=B69DD74875FC8B0B61E55FDC89126479>) and the ICME list of Richardson and Cane (<http://www.srl.caltech.edu/ACE/ASC/DATA/level3/icmetable2.htm>). Data for the produced solar flares were obtained from the *Geostationary Operational Environmental Satellite* (GOES) measurements ([https://www.ngdc.noaa.gov/stp/space-weather/solar-data/solar-features/solar-flares/x-rays/goes/xrs/goes-xrs-report\\_2015.txt](https://www.ngdc.noaa.gov/stp/space-weather/solar-data/solar-features/solar-flares/x-rays/goes/xrs/goes-xrs-report_2015.txt)) and from the website <http://www.solarmonitor.org>.

Cosmic-ray data hourly corrected for pressure and efficiency were obtained from the High Resolution Neutron Monitor Database (NMDB) (<http://www.nmdb.eu>). This database contains high-resolution CR data recorded at about 50 neutron monitors located at different locations on Earth, which are characterized by different cutoff rigidities. The FD database of the IZMIRAN CR group of the Russian Academy of Science was very useful because it provides information on the different parameters of the studied events (<http://spaceweather.izmiran.ru/eng/dbs.html>).

For the geomagnetic Dst index, provisional data from the World Data Center for Geomagnetism ([http://wdc.kugi.kyoto-u.ac.jp/dst\\_provisional/201506/index.html](http://wdc.kugi.kyoto-u.ac.jp/dst_provisional/201506/index.html)) were used. For the interplanetary parameters, we also obtained data from OMNIWeb (<http://omniweb.gsfc.nasa.gov>). The magnetic field and solar wind data are provided from the ACE, Wind, IMP8, and Geotail spacecraft for the time period from 1995 until the present. One-minute (1 min) resolution AE-index and SYM-H data were computed at the World Data Center for Geomagnetism and Space Magnetism at Kyoto University.

A series of solar events, *i.e.* solar flares and CMEs, were observed from 18 June to 25 June 2015. These events were produced in Active Region AR 2371 (Figure 1), which was the most energetic region of the four active regions that appeared on the Sun in this period. The observed FDs of June 2015 were the most severe events that occurred during Solar Cycle 24. It is noted that this event presents an unusual structure of the recorded FDs, since a second FD is observed within the first in less than three days. A similar event occurred in June 2005 (Papaioannou *et al.*, 2009).

### 3. Solar Activity

During the time period from 17 June to 29 June 2015, 25 C-class and 4 M-class flares were produced from the powerful AR 2371, which dominated the solar activity during that period.

To be more precise, the four most intense solar flares (M-class flares) from AR 2371 were recorded on

- i) June 20, when an M1.0-class flare started around 6:28 UT, with a peak time around 6:48 UT and a stop time at 7:09 UT;
- ii) June 21, when an M2.0-class flare began at 1:02 UT, peaked at 1:42 UT and stopped at 2:00 UT;
- iii) June 22, when an M6.6-class flare appeared at 17:39 UT with a peak time at 18:23 UT and an end time at 18:51 UT; and
- iv) June 25, when an M7.9-class flare started at 8:02 UT, peaked at 8:16 UT and stopped at 9:05 UT.

Furthermore, on June 18 at 17:25 UT, a halo CME (from now on, CME-2) with a linear speed of 1305 km/s was captured by the C2 coronagraph of the SOHO Observatory ([https://cdaw.gsfc.nasa.gov/CME\\_list/](https://cdaw.gsfc.nasa.gov/CME_list/)). On the next day, June 19 at 06:42 UT, a second CME (from now on, CME-3) was observed emerging from the Sun with a linear speed of 584 km/s. Two days later, on June 21 at 02:36 UT, a third more intense halo CME (from now on, CME-4) was recorded by the SOHO/LASCO coronagraph (Figure 2, middle panel) with an estimated linear speed of 1366 km/s. It propagated in the interplanetary space as an ICME and reached the Earth's neighborhood on June 22, around 17:59 UT. Additionally, on June 22 at 18:36 UT, a fourth CME (from now on, CME-5) was observed, being characterized by a linear speed of 1209 km/s (Figure 2, lower panel), while it also propagated as an ICME in space and reached the Earth's vicinity on June 24, around 12:57 UT. Last but not least, a fifth halo CME was recorded on June 25 at 08:36 UT. Except for two additional partial-halo CMEs that were also recorded by the LASCO coronagraph on 18 June and on 26 June, which did not really influenced the Earth, there is no other remarkable solar event for the remaining month.

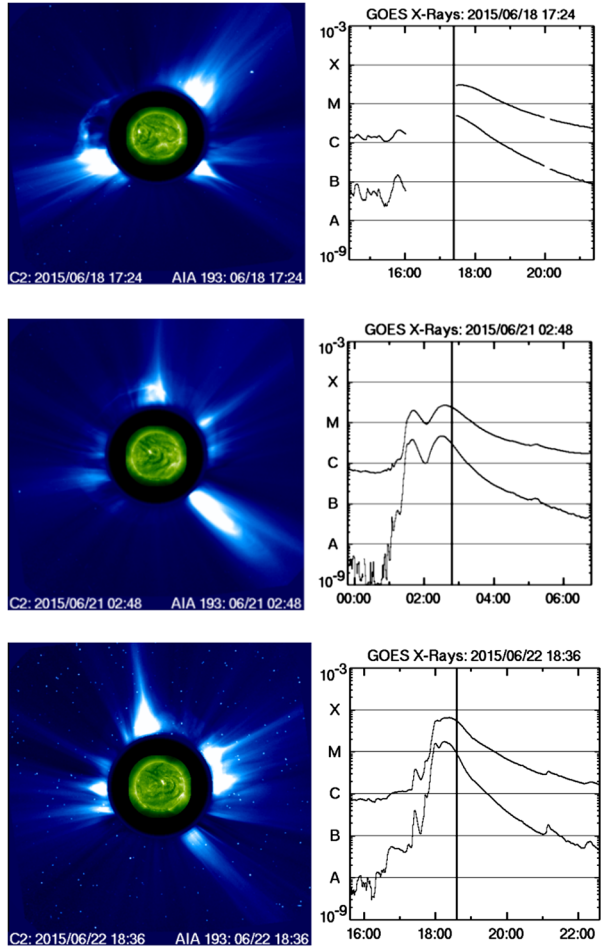
All this information on CMEs is briefly summarized in Table 1. The first column presents the serial number of each CME, the second and the third columns indicate the date and the time captured by the SOHO/LASCO coronagraph, respectively, and the fourth and the fifth columns display their shock arrival date and time on Earth. The CME type (halo/partial halo) is recorded in the sixth column of Table 1 and their linear velocities in Column 7.

### 4. Cosmic-ray Activity

In the second half of June 2015, the solar activity was very intense, as we described, since a number of CMEs and flares were produced. The result was a very interesting and unusual formulation of the galactic CR flux, which appeared as a series of FDs (Lingri *et al.*, 2016).

According to the National Oceanic and Atmospheric Administration (NOAA, <http://www.noaa.gov>), FDs are abrupt decreases in background galactic CR intensity as observed by neutron monitors, while Forbush effects describe changes with an amplitude lower than 3% (*e.g.* Belov *et al.*, 2001). In our case, decreases with amplitudes lower than 3% are not included in the presented lists (<https://www.ngdc.noaa.gov/stp/solar/cosmic.html>). The event we studied is intriguing because of the unusual structure of the FD on June 24, since a second FD was observed less than three days after the first. The time profiles of the CR intensity

**Figure 2** Upper panels: CME-2 on 18 June 2015, as seen by the LASCO C2 coronagraph (left panel) and the increase in X-ray component as recorded by the GOES satellites (right panel). The middle and lower panel present the same for CME-4 and CME-5, respectively.



recorded at the Oulu (cutoff rigidity 0.81 GV), Irkutsk (cutoff rigidity 3.64 GV), Rome (cutoff rigidity 6.27 GV), and Athens (cutoff rigidity 8.53 GV) neutron monitor stations are given in Figure 3. The CR intensity measurements for each station were normalized to the average CR value the day before the start of the event, *i.e.* June 18. Specifically, the data were normalized to zero according to the following relation:

$$I_{\text{norm}}^{(n)} = \frac{I_n - \bar{I}}{I_n}, \tag{1}$$

where  $\bar{I}$  is the mean value of the CR intensity taking into account 24 CR values starting at 00:00 UT of June 18, where the CR behavior can still be characterized as normal. The variable  $I_n$  ( $n = 1, \dots, N$ ) represents the CR intensity of the  $N$  values as recorded by the neutron monitors, while  $I_{\text{norm}}^{(n)}$  are the corresponding normalized values, quoted as a percentage.

The onset time of the first FD that can be identified by the SSC recorded at 18:33 UT on 22 June 2015 as a result of the arrival of the CME-4 shock at the Earth’s magnetosphere is indicated in Figure 3. To be more precise, the Oulu neutron monitor station recorded

**Table 1** Characteristics of the ejected CMEs from 18 June to 26 June 2015 (taken from the SOHO/LASCO CME Catalog [cdaw.gsfc.nasa.gov/CME\\_list](http://cdaw.gsfc.nasa.gov/CME_list)) and the associated ICME shock arrival date and time (taken from the CME Arrival Time Scoreboard of NASA CCMC <https://kauai.cmc.gsfc.nasa.gov/CMEscoreboard/PreviousPredictions/2015;jsessionid=B69DD74875FC8B0B61E55FDC89126479>).

| CME#  | Recorded date | Recorded time (UT) | Arrival date | Arrival time | Type         | Linear velocity (km/s) |
|-------|---------------|--------------------|--------------|--------------|--------------|------------------------|
| CME-1 | 18.06.2015    | 01:25              | N/A          | N/A          | Partial Halo | 1714                   |
| CME-2 | 18.06.2015    | 17:24              | 21.06.2015   | 15:40        | Halo         | 1305                   |
| CME-3 | 19.06.2015    | 06:42              | 22.06.2015   | 04:51        | Halo         | 584                    |
| CME-4 | 21.06.2015    | 02:36              | 22.06.2015   | 17:59        | Halo         | 1366                   |
| CME-5 | 22.06.2015    | 18:36              | 24.06.2015   | 12:57        | Halo         | 1209                   |
| CME-6 | 25.06.2015    | 08:36              | 27.06.2015   | 03:30        | Halo         | 1627                   |
| CME-7 | 26.06.2015    | 13:25              | N/A          | N/A          | Partial Halo | 563                    |

a decrease of 8.6% at 04:00 UT on 23 June 2015, while the Irkutsk, Rome, and Athens stations recorded a decrease of 7.5% at 15:00 UT, 5.5% at 18:00 UT, and 5.2% at 21:00 UT, respectively.

After the minimum value of the GCR intensity on 23 June 2015, a very short recovery phase started. Its duration ranged from few hours to almost one day, and it was followed by a second FD that began at around 12:00 UT on 24 June 2015 and reached the value of 5.5% at 23:00 UT on the same day at Oulu station. The respective values for the Irkutsk, Rome, and Athens stations were 4.6% at 18:00 UT, 3.3% at 21:00 UT, and 3.6% at 21:00 UT on 24 June 2015. Finally, the usual recovery came after the event. The connection between the two FDs and the incoming CMEs is also depicted in the same figure.

The behavior of the CR intensity as recorded by several neutron monitor stations of the worldwide network with different cutoff rigidities is depicted in Figure 4. Cosmic ray intensity variations from polar (upper panel), median latitude (medium panel), and low latitude (lower panel) stations are illustrated in this figure. The stations were classified according to their rigidity into the following three groups:

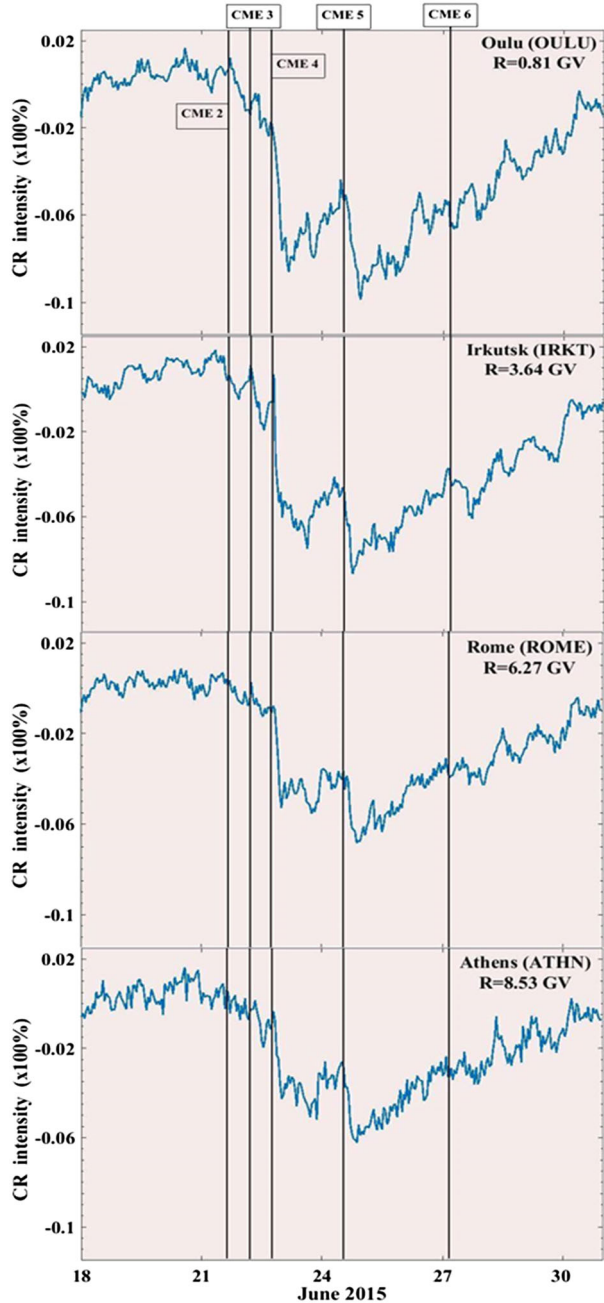
- i) (0–2) GV (TERA, FSMT, THUL, MCMU, TXBY, MRLK, APTY, OULU, YKTK);
- ii) (2–5) GV (KIEL2, NEWK, DOUR, IRKT, LMKS, YUNG, BKSJ);
- iii) (5–9) GV (ROME, CALM, NANM, MXCO, ATHN).

For polar, mid-, and low-latitude stations, respectively. This classification was used in order to verify that the event was clearly recorded all over the world and by almost all the stations, but with different amplitude. The characteristics of the stations used in this work as well as the amplitude of the first and second FDs are given in Table 2.

This table shows that the selected neutron monitor stations cover a wide range of cutoff rigidities, from 0.01 GV to 8.53 GV, including polar, mid-, and low-latitude stations. This underlines the importance of the event because it has been clearly recorded by all the neutron monitor stations around the world within the rigidity range described before.

A detailed study of Table 2 and Figure 4 shows that the recorded FD amplitudes are well related to the cutoff rigidity of the stations. For the group of polar stations, different recorded FD amplitudes were noted that ranged for the first FD from 9.5%, at THUL neutron monitor station (0.30 GV) to the smallest one of 7.3% at TXBY station (0.48 GV). For the second FD, the greatest decrease of 4.9% was registered at APTY (0.65 GV), while the smallest decrease of 3.6% was recorded at FSMT neutron monitor (0.30 GV). The average

**Figure 3** Time profiles of the CR intensity as recorded by the neutron monitors of Oulu, Irkutsk, Rome, and Athens along with the CME arrivals.



amplitude value for the first and the second FD at the polar stations was 8.4% and 4.3%, respectively.

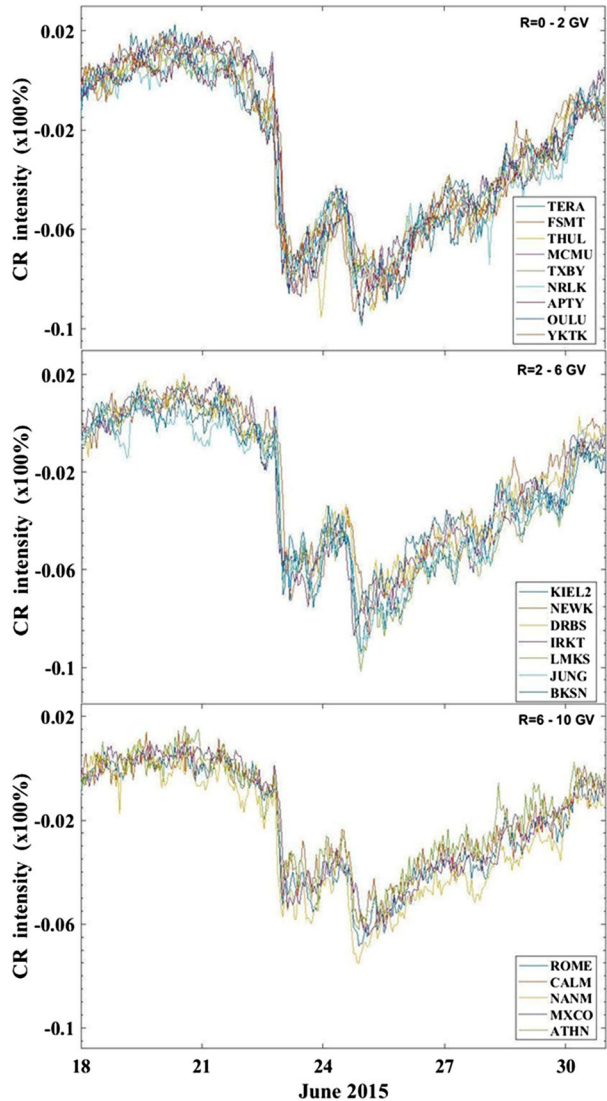
Continuing the study for the mid-latitude stations, the greatest amplitudes for the two FDs were recorded at KIEL2 (2.36 GV) and at LMKS (3.84 GV) and were found to be equal to 7.6% and 5.7%, respectively. The lower amplitude was 6.3% for the first and 4.4%

**Table 2** Characteristics of the neutron monitor stations together with the FD amplitudes recorded by each station.

| A/A | NM stations (abbr.)<br>country    | Rigidity<br>(GV) | Geographic coordinates<br>lat./long. | Altit.<br>(m) | 1st FD<br>ampl. (%) | 2nd FD<br>ampl. (%) |
|-----|-----------------------------------|------------------|--------------------------------------|---------------|---------------------|---------------------|
| 1   | Apatity (APTY)<br>Russia          | 0.65             | 67.57° N/33.40° E                    | 181           | 8.5                 | 4.9                 |
| 2   | Athens (ATHN)<br>Greece           | 8.53             | 37.97° N/23.78° E                    | 260           | 5.2                 | 3.6                 |
| 3   | Baksan (BKSN)<br>Russia           | 5.70             | 43.28° N/42.69° E                    | 1700          | 6.9                 | 4.4                 |
| 4   | Dourbes (DRBS)<br>Belgium         | 3.18             | 50.10° N/4.60° E                     | 225           | 6.3                 | 4.4                 |
| 5   | Fort Smith (FSMT)<br>Canada       | 0.30             | 60.02° N/111.93° W                   | 180           | 7.8                 | 3.6                 |
| 6   | Guadalajara (CALM)<br>Spain       | 6.95             | 40.33° N/3.90° W                     | 708           | 5.0                 | 3.8                 |
| 7   | Irkutsk (IRKT)<br>Russia          | 3.64             | 52.47° N/104.03° E                   | 435           | 7.5                 | 4.6                 |
| 8   | Jungfrauoch (JUNG)<br>Switzerland | 4.49             | 46.55° N/7.98° E                     | 3570          | 7.1                 | 5.6                 |
| 9   | Kiel (KIEL2)<br>Germany           | 2.36             | 54.34° N/10.12° E                    | 54            | 7.6                 | 5.7                 |
| 10  | Lomnický štít (LMKS)<br>Slovakia  | 3.84             | 49.20° N/20.22° E                    | 2634          | 7.2                 | 5.7                 |
| 11  | McMurdo (MCMU)<br>Antarctica      | 0.30             | 77.90° S/166.60° E                   | 48            | 8.7                 | 4.2                 |
| 12  | Mexico (MXCO)<br>Mexico           | 8.28             | 19.33° N/260.82° E                   | 2274          | 5.4                 | 3.4                 |
| 13  | Newark (NEWK)<br>USA              | 2.40             | 39.68° N/75.75° W                    | 50            | 7.3                 | 5.3                 |
| 14  | Nor-Amberd (NANM)<br>Armenia      | 7.10             | 40.22° N/44.15° E                    | 2000          | 6.0                 | 4.1                 |
| 15  | Norilsk (NRLK)<br>Russia          | 0.63             | 69.26° N/88.50° E                    | 0             | 7.8                 | 3.7                 |
| 16  | Oulu (OULU)<br>Finland            | 0.81             | 65.05° N/25.47° E                    | 15            | 8.6                 | 5.5                 |
| 17  | Rome (ROME)<br>Italy              | 6.27             | 41.86° N/12.47° E                    | 0             | 5.5                 | 3.3                 |
| 18  | Terre Adelie (TERA)<br>Antarctica | 0.01             | 66.65° S/140.00° E                   | 32            | 8.6                 | 4.5                 |
| 19  | Thule (THUL)<br>Greenland         | 0.30             | 76.50° N/68.70° W                    | 26            | 9.5                 | 4.1                 |
| 20  | Tixie Bay (TXBY)<br>Russia        | 0.48             | 71.36° N/128.54° E                   | 0             | 7.3                 | 3.9                 |
| 21  | Yakutsk (YKTK)<br>Russia          | 1.65             | 62.01° N/129.43° E                   | 105           | 8.5                 | 4.4                 |

for the second FD, both recorded at DRBS neutron monitor station (3.18 GV). The average value of the decrease in this category of stations was 7.1% for the first FD and 5.1% for the second one.

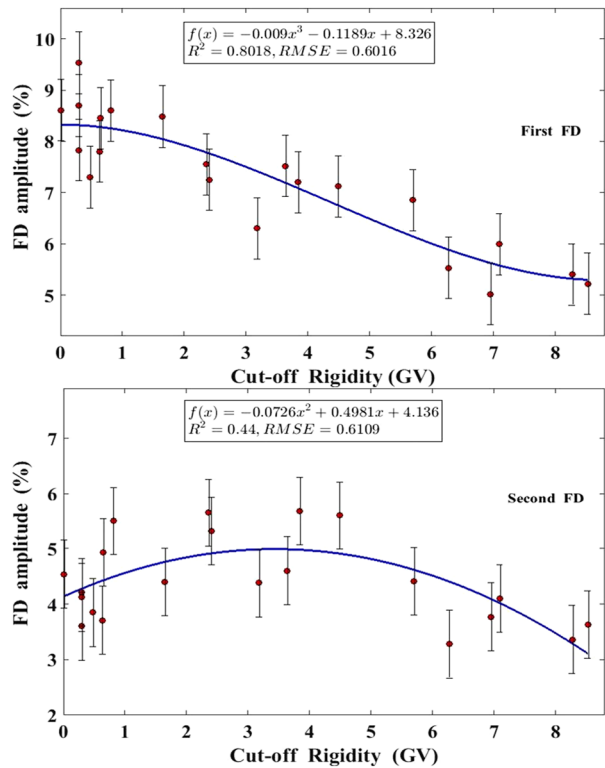
**Figure 4** CR intensity variations from 22 June to 30 June 2015, as recorded by the ground-based neutron monitor stations located at polar (*upper panel*), mid (*middle panel*), and high (*lower panel*) latitudes.



Finally, the low-latitude stations saw a smaller variation in the registered number of particles. The average value of the two FDs in this case was 5.4% and 3.6%, respectively, with the greatest values (6.0%–4.1%) to be recorded at NANM (7.10 GV) and the lowest values (5.0%–3.3%) at CALM and ROME neutron monitor stations, respectively. From this analysis we conclude that the two FDs of CR intensity in June 2015 were recorded with significant amplitude throughout the examined cutoff rigidity range, from 0.01 GV to 8.53 GV.

It is known that during a FD, a decrease in CR intensity with amplitude inversely proportional to the cutoff rigidity related to the location of the CR station is observed (Lockwood, 1971; Lingri *et al.*, 2016). The dependence between the decrease in CRs and the cutoff rigidity of each station, which in turn is related to each station's geographical latitude, is shown in Figure 5. In particular, the upper panel shows the first FD that occurred on June 22, while

**Figure 5** FD amplitude as a function of the cutoff rigidity of different stations for the first (*upper panel*) and second (*lower panel*) FDs. The *error bars* represent the root mean square error.



the lower panel shows the second FD on June 24. By performing a regression analysis of the given data, we found that the best fit describing the relation between the FD amplitude and the cutoff rigidity of the used stations was a polynomial fit. This choice was made using the statistics  $R^2$  – criterion, which takes values between zero and one. The closer to one the value, the better the fit. This criterion can be very well applied to the first FD, in contrast to the second FD, where more values seem to deviate from the model. We also calculated the root mean square errors (RMSE), which are depicted with the error bars in the diagrams of Figure 5.

The upper panel of Figure 5, for the first FD, clearly follows the model described above, that is to say, the lower the cutoff rigidity, the greater the variation in the recorded CR intensity (Lockwood, 1971). It is interesting that in the present event, the second FD seems to deviate from the standard model. We note that the amplitude of the second FD was calculated by setting the previous local maximum as the point of reference (see CME-5 in Figure 3). The explanation for this behavior is due to the nature of the event itself since a second FD begins almost one day after the first minimum, interrupting the recovery process of the first FD. Thus, no neutron monitor station has yet fully recovered, and the recovery process will be different for each station. It seems that the mid-latitude stations (cutoff rigidities around 4.50 GV) have been substantially recovered and recorded higher FD amplitudes.

We also note that the second FD is less affected by the cu-off rigidity changes, and the range of the FD amplitudes is significantly smaller than that of the first FD. This behavior can also be explained as due to the recovery process as mentioned above. The same correlations have also been observed in a number of FD events (Lingri *et al.*, 2016). In addition, our results for the first FD agree very well with the work of Bachelet, Balata, and Iucci (1965)

on the latitudinal behavior of CRs at mid-latitude stations, which is important for the modification of the latitude curves. Finally, we conclude that the CME shock arrivals between June 18 and 22, 2015 influenced the CR intensity in a dynamic way, as was recorded by multiple neutron monitor stations with different rigidities (Figures 3, 4, 5).

## 5. The Geomagnetic Storm

As the event of June 2015 was characterized as a geoeffective solar event (Piersanti *et al.*, 2017), an extended study on the geomagnetic indices causing GSs was also performed. The variations in  $K_p$  and the Dst indices for the period 18–30 June 2015 are presented in the lower panel of Figure 6, while the variation of the CRs of rigidity 10 GV is given in the upper panel of the same figure. Using the global survey method (GSM), the CR density and the first harmonic of anisotropy for the CRs of 10 GV rigidity were calculated. The rigidity of 10 GV is close to the effective rigidity of the particles being recorded by the neutron monitors of the worldwide network (Belov *et al.*, 2005; Asipenka *et al.*, 2009).

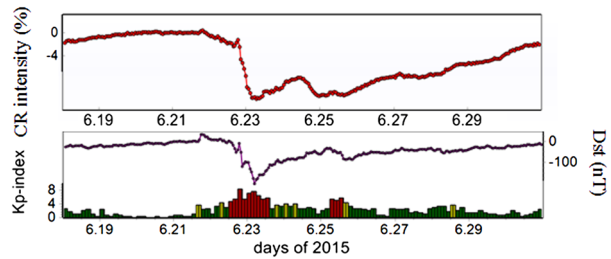
The upper panel of this figure confirms that the first FD started in the afternoon of June 22 and within almost one day, reached the value of 8.4% at the rigidity of 10 GV, while it was followed by a short and slow recovery. Two days after this FD, on June 24 at around 23:00 UT, a second FD, characterized by a decrease of 4.0% in the CR intensity, started. Finally, a second recovery phase took place.

The lower panel of this figure shows that the increase in  $K_p$  index preceded on 22 June 2015 at 18:00 UT, reaching the value of eight, which corresponds to a severe G4 GS. The  $K_p$  index continued with high values until June 23 at 05:00–6:00 UT, indicating a second G4 GS. According to NOAA, GSs can be classified by their intensity. This process is based on the  $K_p$  index and is known as the NOAA GS Space Weather Scale, or G-Scale (<http://www.swpc.noaa.gov/noaa-scales-explanation>). This scale is extended from “Minor” to “Severe” storms for  $K_p$  index values of five and nine, respectively. Therefore, the G4 storm corresponds to the  $K_p = 8$  value, characterized as “Severe”, and the G2 storm to the  $K_p = 2$  value, characterized as “Moderate”. A similar behavior was observed in the values of the Dst index with a first minimum of  $-124$  nT and a second of  $-204$  nT, in coincidence with the variation of the  $K_p$  index. Comparing the  $K_p$  values with the CRs at 10 GV obtained from the IZMIRAN database (Figure 6, upper panel), we note that the maximum of the  $K_p$  index coincides with the minimum of the CR intensity. The second minimum of the Dst index  $-204$  nT was recorded (preliminary data) on 23 June 2015 at 05:00–06:00 UT, about four hours after the minimum of the CR intensity. The development of the GSs was additionally confirmed from the sudden decreases in Dst index (e.g. Gromova *et al.*, 2016), as illustrated in the upper curve in the lower panel of Figure 6.

After this, the geomagnetic activity returned to the quiet – unsettled level, except for temporary active conditions such as on June 25, where a moderate G2 storm was recorded. This storm seems to be associated with CME-6 on 25 June 2015.

By exploring the relation between the Dst index and the CR variation (Figures 3 and 6), it is clear that the GS is strongly connected with the CR intensity decrease. The GS and the FD behavior began by evolving in a similar way, but the recovery profiles of the two parameters (Dst and CR intensity) were different, probably because of the CME-5 arrival, which interrupted the recovery phase of the first FD, causing the second decrease in CR intensity. These results are in agreement with those described by Aslam and Badruddin (2017).

**Figure 6** Variation in CR intensity at 10 GV (*upper panel*) and the Dst and Kp indices (*lower panel*) from 18 June to 30 June 2015.



In the FD recovery phase and about ten hours after the Dst minimum, a peak in CR intensity was recorded, indicating a possible magnetospheric effect, as the Dst index reached the value of  $-204$  nT on June 23 at 05:00–06:00 UT (Figure 4). As expected, this peak was observed in the mid- and low-latitude neutron monitor stations, but not in the polar ones. This can be explained as due to the compression of Earth's magnetosphere, which mainly affects the mid-latitude stations. According to a model due to Tsyganenko and Stern (1996) and Plainaki *et al.* (2009), referred to as the Tsyganenko96 model, large cutoff rigidity variations occur during these events, such as the one of 20 November 2003, where an aurora appeared in Athens (lat.  $38^\circ$ , 8.53 GV) for the first time (Belov *et al.*, 2005; Mavromichalaki *et al.*, 2013).

The SSC of 22 June is well identified from the sudden increase in solar wind flow velocity and the proton density that lead to a sudden increase in SYM-H index (Joselyn and Tsurutani, 1990).

From the SYM-H index data, it is apparent that two periods of abrupt escalation of the geomagnetic activity on June 21 and June 22 preceded the storm (Figure 7). Solar wind flow velocity increases and the sudden direction flips of the interplanetary magnetic field result in these intense geomagnetic activity time intervals. From studying either the Dst or the SYM-H index, it is clear that this storm has a dual character. A second sudden decrease succeeds the first, and this rare effect causes a dual GS. This duality can give us information about the connection between the IMF flips and the SYM-H sudden decreases (Piersanti *et al.*, 2017). The two time intervals when the sudden decreases occur and those when the IMF component is proximate located in a negative value are in a good agreement.

These time intervals coincide with those for the AE index at high latitudes. The AE index exhibits sudden and large fluctuations corresponding to the SYM-H index decrease time intervals (Liu *et al.*, 2015). As a result, the primary AE index outbreak is directly correlated with the SSC, and the subsequent ones are correlated with the resulting SYM-H index decreases. The magnetic field component  $B_z$ , the solar wind flow, the AE, and the SYM-H index for the examined time period are presented in Figure 7. The red lines indicate the CME shock arrivals, and the blue lines the minimum of the geomagnetic indices.

## 6. Interplanetary Conditions

During this energetic phenomenon, the interplanetary parameters did not remain unaffected. The mean interplanetary magnetic field reached the value of 37.7 nT during the disturbance, while the maximum solar wind velocity was 742 km/s. The CR anisotropy in the ecliptic plane was affected by the disturbance and reached the maximum value of 3.4%, calculated using the GSM method, as is shown in Figure 8. From this figure it is clear that after the first SSC arrival, the anisotropy vector changed its direction immediately. From this time, when

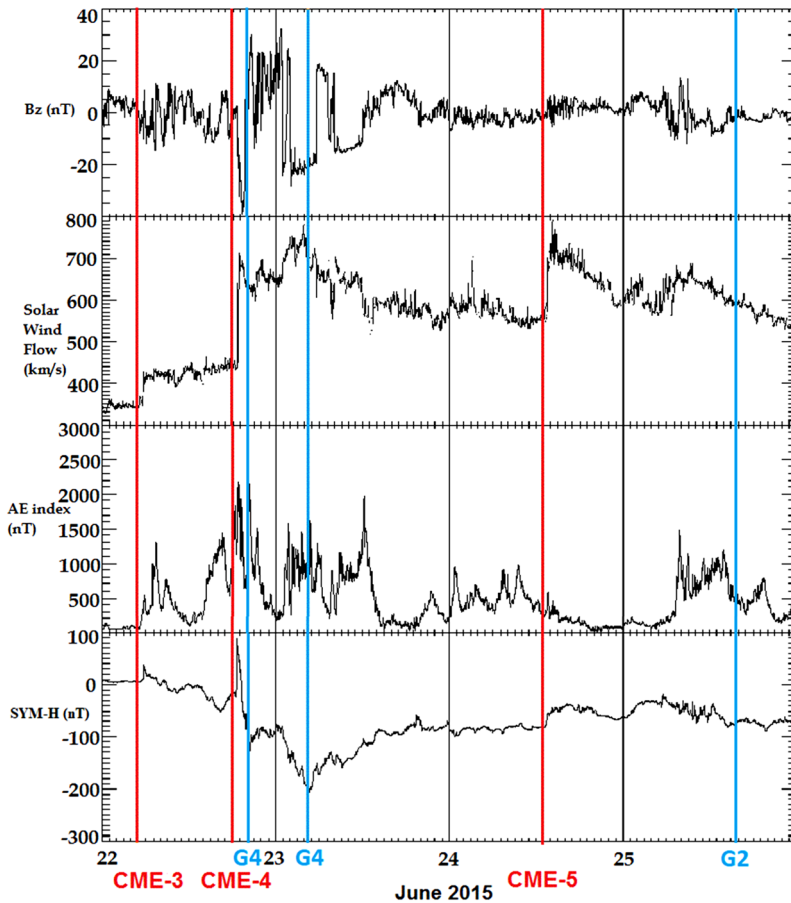
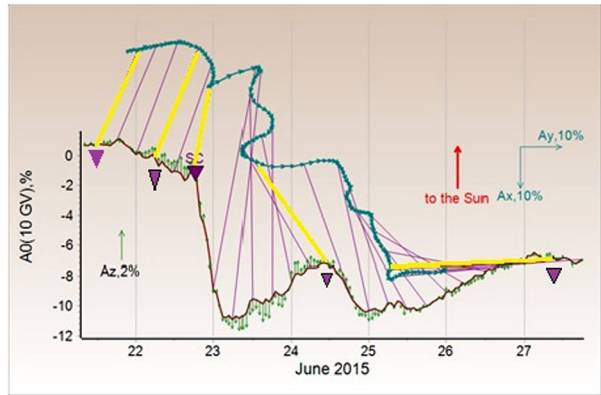


**Figure 7** Time profiles of the magnetic field  $B_z$  component, the solar wind velocity, the AE index, and the SYM-H index from 22 June to 25 June 2015. The vertical red lines indicate the CME shock arrivals, and the blue lines indicate the geomagnetic storms ([omniweb.gsfc.nasa.gov](http://omniweb.gsfc.nasa.gov)).

each one of the CMEs reached the Earth's orbit, significant changes were observed and the status became complicated indeed. It has to be noted that in the anisotropy vector, there were significant changes by all the CMEs that reached the Earth and did not affect the CR intensity in the same way. For instance, when CME-6 reached Earth on 27 June 2015, the anisotropy vector changed significantly, while the CR intensity was affected by a variation of only 1.4% at 10 GV, as presented in Figure 8.

Moreover, for a better overview of these event characteristics recorded at different neutron monitor stations of the worldwide network, it is important to estimate the particle trajectories in the near-Earth interplanetary space. Using a numerical back-tracing technique and a number of neutron monitors around the globe, we calculated the proton trajectories inside the geomagnetic field, covering a wide range of particle energies. An extended representation of the Earth's magnetic field was realized by applying the Tsyganenko96 model. Assigning the term "neutron monitor asymptotic cone" to the set of allowed trajectories traces at the altitude of 80 km above the Earth surface for this specific station, the magnetospheric windows of six neutron monitors (NRLK, APTY, NEWK, LMKS, BKSJ, and

**Figure 8** Anisotropy variation in cosmic ray intensity at the ecliptic plane during the period of 21 June to 27 June 2015. The purple triangles indicate the time at which the CMEs reached Earth, and the yellow lines show the anisotropy vectors at this exact time.



ATHN) were defined. These six neutron monitors were selected as they span the range of the existing cutoff rigidities. The asymptotic cones for each station were calculated at five different time stamps that correspond to five phases of the event:

- $T_{\text{nor}}$ : the two-day time before the start of the event with low geomagnetic activity ( $K_p = 0$ );
- $T_{\text{min1}}$ : the time of the first minimum with high geomagnetic activity;
- $T_{\text{rec1}}$ : the time during the recovery of the first FD with medium geomagnetic activity ( $K_p = 3$ );
- $T_{\text{min2}}$ : the time of the second FD minimum;
- $T_{\text{rec2}}$ : the time during the recovery of the second FD with low geomagnetic activity ( $K_p = 0$ ).

The time evolution of the asymptotic cones of the selected stations for these time stamps is presented in Figure 9. The asymptotic cones of polar and high-latitude stations are highly affected by the magnetospheric structure during this event. Only in the presented case of the low energetic particles, the asymptotic cones of stations with cutoff rigidities from 2 to 4 GV seem to be affected by the event. On the other hand, the asymptotic cones of stations with higher cutoff rigidities appear nearly unaffected by the geoeffective event.

In general, by examining the asymptotic cones for each station separately, we found the trajectories of the low-energy particles to be more affected by the arrival of the CMEs than the corresponding trajectories of the high-energy particles. The differences in the traces as the event evolved in time are unnoticeable, especially above energies of 10 GV.

## 7. Conclusions

We analyzed the CR and geomagnetic response to a series of solar events from 9 June to 25 June 2015. The study revealed a complex geoeffective event, for which our conclusions can be summarized as follows:

- Several M-class flares originating from the same AR were observed, along with a series of seven halo and partial-halo CMEs from the Sun, five of which reached Earth within about six consecutive days.
- A significant double FD was recorded by all the neutron monitor stations with an amplitude of 8.4% on June 22 and 4.0% on June 24, for CRs of 10 GV.

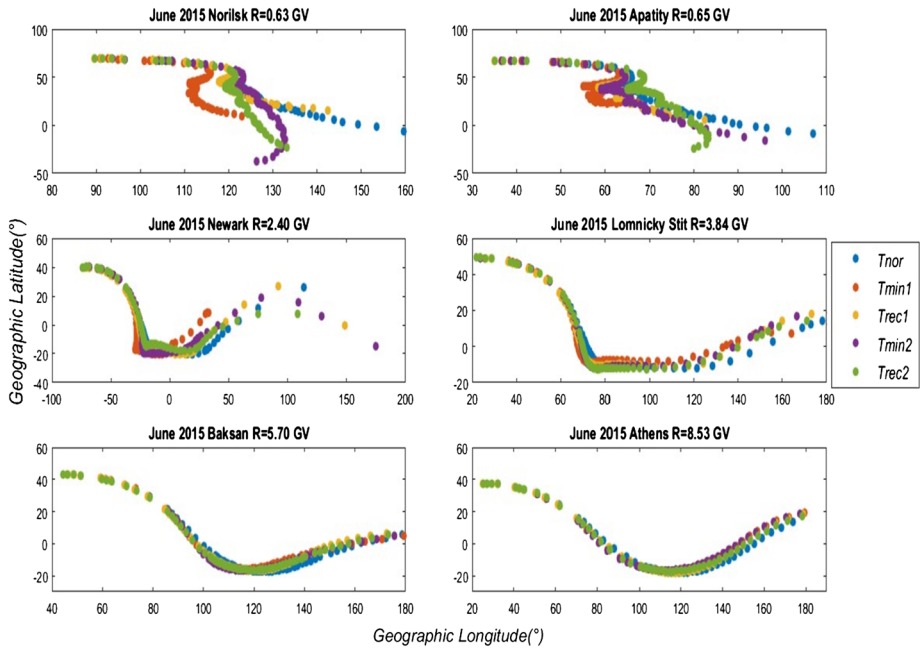


**Figure 9** Time evolution of the asymptotic cones during the event of June 2015 for NRLK, APTY, NEWK, LMKS, BKSJ, and ATHN neutron monitor stations. The trajectories of the highly energetic particles are presented at the *left side* of the asymptotic cone of each station.

- The  $K_p$  index reached the value of 8 and remained increased before the FD reached its minimum, while the Dst reached its minimum value of  $-204$  nT after the FD minimum.
- A sequence of two intense GSs (G4) took place, as was confirmed by the minimum value of the Dst index and the recorded peak in the recovery phase of the first FD at the polar stations. Furthermore, a moderate GS (G2) appeared after the second minimum of the CR intensity.
- The anisotropy behavior of the CR intensity at the ecliptic plane during this period seems to be very complicated because of a variety of disturbances in interplanetary space. The study of the asymptotic cones during the event confirms the differences of the anisotropy at the polar, mid-, and low-latitude stations.
- Stations with low cutoff rigidity perceive strong changes in their asymptotic directions, whereas stations with high cutoff rigidity present almost no changes in their asymptotic directions during this event. The strongest changes in every station’s cone occurred in the lower energetic particles coming from interplanetary space.

In summary, the study of such events would lead to a better understanding of the Sun’s variability and the terrestrial impact. The analysis of other events with the same peculiarities will help not only in this direction, but to generally advance space weather research.

**Acknowledgements** Special thanks to the colleagues of the NM stations (<http://www.nmdb.eu>) for kindly providing the cosmic-ray data used in this study in the frame of the high-resolution neutron monitor database NMDB, funded under the European Union’s FP7 Program (contract no. 213007). Thanks are due to the IZMIRAN group of the Russian Academy of Sciences for kindly providing Forbush decrease data. The co-author D. Lingri thanks the General Secretariat for Research and Technology (GSRT) and the Hellenic Foundation for Research and Innovation (HFRI) of the Greek Ministry of Education for supporting her PhD fellowship.

Thanks are also due to the anonymous referee for useful suggestions that improved this manuscript significantly.

**Conflict of Interest** The authors declare that they have no conflicts of interest.

## References

- Akasofu, S.I., Ahn, B.H., Kamide, Y., Allen, J.H.: 1983, A note on the accuracy of the auroral electrojet indices. *J. Geophys. Res.* **88**, 5769. [DOI](#).
- Asipenka, A.S., Belov, A.V., Eroshenko, E.A., Klepach, E.G., Oleneva, V.A., Yanke, V.G.: 2009, Interactive database of cosmic ray anisotropy (DB-A10). *Adv. Space Res.* **43**, 708. [DOI](#).
- Aslam, O.P.M., Badruddin: 2017, Study of the geoeffectiveness and galactic cosmic-ray response of VarSITI-ISEST campaign events in Solar Cycle 24. *Solar Phys.* **292**, 17. [DOI](#).
- Bachelet, F., Balata, P., Iucci, N.: 1965, Some properties of the radiation recorded by the IGY cosmic-ray neutron monitors in the lower atmosphere. *Nuovo Cimento A* **40**, 250. [DOI](#).
- Badruddin: 2006, Transient perturbations and their effects in the heliosphere, the geo-magnetosphere, and the Earth's atmosphere: space weather perspective. *J. Astrophys. Astron.* **27**, 209. [DOI](#).
- Bartels, J.: 1949, The standardized index Ks and the planetary index Kp. *IATME Bull.* **12b**, 97.
- Belov, A.V., Eroshenko, E.A., Oleneva, V.A., Struminsky, A.B., Yanke, V.G.: 2001, What determines the magnitude of Forbush decreases? *Adv. Space Res.* **27**, 625. [DOI](#).
- Belov, A., Baisultanova, L., Eroshenko, E., Mavromichalaki, H., Yanke, V., Pchelkin, V., Plainaki, C., Mariatos, G.: 2005, Magnetospheric effects in cosmic rays during the unique magnetic storm on November 2003. *J. Geophys. Res.* **110**, A09. [DOI](#).
- Cane, H.V.: 2000, Coronal mass ejections and Forbush decreases. *Space Sci. Rev.* **93**, 55. [DOI](#).
- Davis, T.N., Sugiura, M.: 1966, Auroral electrojet activity index *AE* and its universal time variations. *J. Geophys. Res.* **71**, 785. [DOI](#).
- Eroshenko, E., Belov, A., Mavromichalaki, H., Mariatos, G., Oleneva, V., Plainaki, C., Yanke, V.: 2004, Cosmic ray variations during the two great bursts of solar activity in the 23rd solar cycle. *Solar Phys.* **224**, 345. [DOI](#).
- Gonzalez, W.D., Joselyn, J.A., Kamide, Y., Kroehl, H.W., Rostoker, G., Tsurutani, B.T., Vasyliunas, V.M.: 1994, What is a geomagnetic storm? *J. Geophys. Res.* **99**, 5771. [DOI](#).
- Gromova, L.I., Kleimenova, N.L., Levitin, A.E., Gromov, S.V., Dremukhina, L.A., Zelinskii, N.R.: 2016, Daytime geomagnetic disturbances at high latitudes during a strong magnetic storm of June 21–23, 2015: the storm initial phase. *Geomagn. Aeron.* **56**, 281. [DOI](#).
- Harrison, R.A.: 1995, The nature of solar-flares associated with coronal mass ejection. *Astron. Astrophys.* **304**, 585.
- Hundhausen, A.J.: 1999, Coronal mass ejections. In: Strong, K.T., Saba, J.L., Haisch, B.H., Schmelz, J.T. (eds.) *The Many Faces of the Sun: A Summary of the Results from NASA's Solar Maximum Mission*, Springer, New York, 143. [DOI](#).
- Joselyn, J.A., Tsurutani, B.T.: 1990, Geomagnetic sudden impulses and storm sudden commencements: a note on terminology. *Eos Trans. AGU* **71**, 1808. [DOI](#).
- Kamide Y., Kusano K.: 2015, No major solar flares but the largest geomagnetic storm in the present solar cycle. *Space Weather* **13**, 365. [DOI](#).
- Kudela, K., Storini, M., Hofer, Y.M., Belov, A.: 2000, Cosmic rays in relation to space weather. *Space Sci. Ser. ISSI* **10**, 153. [DOI](#).
- Kudela, K., Brenkus, R.: 2004, Cosmic ray decreases and geomagnetic activity: list of events 1982–2002. *J. Atmos. Solar-Terr. Phys.* **66**, 112. [DOI](#).
- Kumar, A., Badruddin: 2014, Interplanetary coronal mass ejections, associated features, and transient modulation of galactic cosmic rays. *Solar Phys.* **289**, 2177. [DOI](#).
- Lingri, D., Mavromichalaki, H., Belov, A., Eroshenko, E., Yanke, V., Abunin, A., Abunina, M.: 2016, Solar activity parameters and associated Forbush decreases during the minimum between Cycles 23 and 24 and the ascending phase of Cycle 24. *Solar Phys.* **291**, 1025. [DOI](#).
- Liu, Y.D., Hu, H., Wang, R., Yang, Z., Zhu, B., Liu, Y.A., Luhmann, J.G., Richardson, J.D.: 2015, Plasma and magnetic field characteristics of solar coronal mass ejections in relation to geomagnetic storm intensity and variability. *Astrophys. J. Lett.* **809**, L34. [DOI](#).
- Livada, M., Lingri, D., Mavromichalaki, H.: 2015, Galactic cosmic ray spectrum of the Forbush decreases of March 2012. In: *Proc. 12th Hel.A.S. Conf.*, vol. 1, p. 12.
- Lockwood, J.A.: 1971, Forbush decreases in the cosmic radiation. *Space Sci. Rev.* **12**, 658. [DOI](#).

- Mavromichalaki, H., Papaioannou, A., Mariatos, G., Papahliou, M., Belov, A., Eroshenko, E., Yanke, V., Stassinopoulos, E.G.: 2007, Cosmic ray radiation effects on space environment associated to intense solar and geomagnetic activity. *IEEE Trans. Nucl. Sci.* **54**, 1089. DOI.
- Mavromichalaki, H., Eroshenko, E., Belov, A., Yanke, V., Mariatos, G., Laoutaris, A., Kontiza, A.: 2013, Magnetospheric cut-off rigidity variations recorded by neutron monitors in the events from 2001 to 2010. Proc. 23rd ECRS. *J. Phys. Conf. Ser.* **409**. DOI.
- Papaioannou, A., Belov, A., Mavromichalaki, H., Eroshenko, E., Oleneva, V.: 2009, The unusual cosmic ray variations in July 2005 resulted from western and behind the limb solar activity. *Adv. Space Res.* **43**, 582. DOI.
- Papaioannou, A., Souvatzoglou, G., Paschalis, P., Gerontidou, M., Mavromichalaki, H.: 2014, *Solar Phys.* **289**, 423. DOI.
- Papailiou, M., Mavromichalaki, H., Eroshenko, E., Belov, A., Yanke, V.: 2012, Precursor effects in different cases of Forbush decreases. *Solar Phys.* **276**, 337. DOI.
- Piersanti, M., Alberti, T., Bemporad, A., Berrilli, F., et al.: 2017, Comprehensive analysis of the geoeffective solar event of 21 June 2015: effects on the magnetosphere, plasmasphere, and ionosphere systems. *Solar Phys.* **292**, 169. DOI.
- Plainaki, C., Belov, A., Eroshenko, E., Mavromichalaki, H., Yanke, V.: 2007, Modeling ground level enhancements: the event of 20 January 2005. *J. Geophys. Res.* **112**, A04. DOI.
- Plainaki, C., Mavromichalaki, H., Belov, A., Eroshenko, E., Yanke, V.: 2009, Neutron monitor asymptotic directions of viewing during the event of 13 December 2006. *Adv. Space Res.* **43**, 518. DOI.
- Sugiura, M.: 1964, *Hourly Values of Equatorial Dst for IGY*, *Annals of the International Geophysical Year* **35**, Pergamon Press, Oxford, 945.
- Tsurutani, B., Lakhina, G.: 2014, An extreme coronal mass ejection and consequences for the magnetosphere and Earth, *EGU General Assembly*, Vienna, id. 3064.
- Tsyganenko, N.A., Stern, D.P.: 1996, Modeling the global magnetic field of the large-scale Birkeland current systems. *J. Geophys. Res.* **101**, 27187. DOI.
- Venkatesan, D., Badruddin: 1990, Cosmic-ray intensity variations in the 3-dimensional heliosphere. *Space Sci. Rev.* **52**, 121. DOI.
- Wanliss, J.A., Showalter, K.M.: 2006, High-resolution global storm index: Dst versus SYM-H. *J. Geophys. Res.* **111**, A02202. DOI.